



Effect of the nearest-neighbor biquadratic interactions on the spin-1 Nagle–Kardar model

Jin-Tao Yang and Ji-Xuan Hou^a

School of Physics, Southeast University, Nanjing 211189, China

Received 11 August 2022 / Accepted 4 November 2022 / Published online 12 November 2022
© The Author(s), under exclusive licence to EDP Sciences, SIF and Springer-Verlag GmbH Germany, part of Springer Nature 2022

Abstract. In this paper, we investigate the effect of the nearest-neighbor biquadratic interactions on the one-dimensional Nagle–Kardar model and study how the interactions affect the the global phase diagram of this generalized model. For the system given in this paper, the mean-field ferromagnetic interactions of strength J competes with the nearest-neighbor interactions of strength K and the biquadratic interaction of strength Δ . Due to the biquadratic coupling, a new ordered state with distinct spin configuration named the stripe ferromagnetic phase emerges. Three regions with different properties are distinguished by the parameter Δ and in each region rich characteristics about different first- and second-order phase transition lines and significant critical points are presented. The triple points and re-entrant phase transitions are also found in the canonical phase diagrams.

1 Introduction

Phase transitions (PTs) are very common in nature. Classic examples are the solid–liquid and liquid–vapor PTs which can be easily demonstrated by water, and ferromagnetic–paramagnetic PT in ferromagnetic substances. A PT is an intense state change of a thermodynamic system with the variations of its parameters like the temperature and the pressure [1–4]. Generally, analytic discontinuities or singularities in the derivatives of the thermodynamic functions (such as the free energy and the Gibbs free energy) of a system with respect to relevant parameters are the typical properties of PT. This characteristic can be utilized to determine the type of PT according to Ehrenfest [5].

Regarding PT phenomena, an old but still complex and variable type of system, Ising model, has received continuous attention from researchers. Among different attractive models, spin systems with competing short- and long-range interactions are of great theoretical interest [6–30]. An early spin model, the so-called Nagle–Kardar (NK) model, is a quite representative example and remains under research. According to Nagle [31], spin models consisting of competing long- and short-range interactions with ferromagnetic and antiferromagnetic preference, respectively, are shown to hold multicritical behaviors. There exists a magnetization transition in the finite temperature field of such a system in a linear spin-1/2 chain. In another work by Kardar [32], a multicritical phase diagram can be observed in an Ising model with mean-field inter-

actions and nearest-neighbor interactions in both one-dimensional space and two-dimensional space.

The Hamiltonian of the NK model including both the specific competitive mean-field ferromagnetic interactions and the short-range antiferromagnetic interactions reads [33]

$$H = -\frac{K}{2} \sum_{i=1}^N (S_i S_{i+1} - 1) - \frac{J}{2N} \left(\sum_{i=1}^N S_i \right)^2, \quad (1)$$

where $S_i = \pm 1$, $K < 0$, $J > 0$ and N is the number of spins. For $d = 1$ dimension, the system exhibits many interesting phenomena such as temperature jump and negative heat capacity in the microcanonical ensemble. In the canonical ensemble, a frontier line separates the ferromagnetic phase and the paramagnetic phase in the phase diagram, while the nearest-neighbor interactions are antiferromagnetic, and a tricritical point appears on that frontier line. Moreover, the system is solved to show ensemble inequivalence that refers to differences between phase diagrams in the canonical and the microcanonical ensemble [33, 34]. The diagram becomes more complex for $d = 2$ dimensions, since the tricritical point separates the above two phase and the antiferromagnetic phase with zero magnetization [35, 36].

Another intriguing research field is the competition of two different forces interacting on similar scales such as two short-range interactions, which can lead to frustration [37]. A prime example called $J_1 - J_2$ model has been well studied in classical and quantum domains [38–44]. It contains two different short-range couplings and can-

^a e-mail: jxhou@seu.edu.cn (corresponding author)

not exhibit any PT in one-dimensional space, which is quite different from the NK model.

In this paper, we extend the one-dimensional NK model in two aspects and study it via the canonical approach to obtain its rich thermodynamical phenomena of phases. One extension is the shift from spin-1/2 model to spin-1 one and the other is the addition of a new nearest-neighbor biquadratic interaction that exists in another classic model called Blume–Emery–Griffiths model [7–9, 16, 45, 46]. The two short-range interactions can be extensively found in the spin systems and lattice-gas mixture [47] and each interaction in the model can be found in some alloys and metallic compounds [48–50]. Due to the presence of the additional interaction, the extended NK model consists of the frustration from two types of short-range interactions on the same scale, and the competition with a mean-field ferromagnetic coupling of a long range. The model should show more interesting and complicated behaviors in phase transitions and phase diagrams.

The rest of the paper is organized as follows. In Sect. 2, we analyze the extended NK model in the canonical ensemble and obtain the free-energy density by means of the transfer-matrix method. In Sect. 3, we show the ground states of the system and discuss the main properties of the phase diagrams with regard to different parameters in the (K, T) plane. Section 4 is reserved for brief conclusion and summarizing.

2 The extended Nagle–Kardar model

Let us start by considering the extended NK model of N spins variable $S_i = -1, 0, +1$. The Hamiltonian of the model is as follows:

$$H = -\frac{J}{2N} \left(\sum_{i=1}^N S_i \right)^2 - \frac{K}{2} \sum_{i=1}^N S_i S_{i+1} - \frac{\Delta}{2} \sum_{i=1}^N S_i^2 S_{i+1}^2, \tag{2}$$

where the parameter J denotes the mean-field long-range coupling and K denotes ferro- or antiferromagnetic nearest-neighbor interaction. Compared with the NK model, the last sum is an additional biquadratic nearest-neighbor coupling with the parameter Δ . Due to the first term of the Hamiltonian, the universality class of the model belongs to mean field and the corresponding critical exponent is $1/2$ [51]. Without losing generality, the parameter J is set to be unity for simplicity in this paper.

If the third term of the Hamiltonian is ignored ($\Delta = 0$), the Hamiltonian returns to the ordinary spin-1 NK model. The addition of nearest-neighbor biquadratic coupling can result in more complex situations and rich phase transitions. If parameters J, K and Δ are set appropriately, we can obtain a system with competing interactions. For instance, the mean-field long-range

coupling prefers ferromagnetic spins as J is positive and the former nearest-neighbor interaction favors antiferromagnetic alignments when $K < 0$, whereas the latter one with parameter $\Delta < 0$ prefers the “0 - and - ± 1 ” stripes. This special preference will generate a new ordered magnetic state that can be named as the stripe ferromagnetic phase graphically.

The characteristics of the model can be calculated analytically in the canonical ensemble, and the partition function is

$$Z(\beta, N) = \sum_{\{S_i\}} e^{-\beta H} = \sum_{\{S_i\}} \exp \left[\frac{\beta J}{2N} \left(\sum_{i=1}^N S_i \right)^2 + \frac{\beta K}{2} \sum_{i=1}^N S_i S_{i+1} + \frac{\beta \Delta}{2} \sum_{i=1}^N S_i^2 S_{i+1}^2 \right], \tag{3}$$

where $\beta = (k_B T)^{-1}$, T is the absolute temperature and k_B is the Boltzmann constant that is set to be unity. Using the Gaussian identity (Hubbard–Stratonovich transformation [9, 16])

$$e^{ba^2} = \sqrt{\frac{b}{\pi}} \int_{-\infty}^{\infty} dx \cdot e^{-bx^2 + 2abx}, \tag{4}$$

the partition function of the system can be rewritten as

$$Z = \sqrt{\frac{\beta J N}{2\pi}} \int_{-\infty}^{\infty} dx \cdot e^{-\frac{\beta J N}{2} x^2} \cdot \sum_{\{S_i\}} \prod_{i=1}^N \exp(\beta \tilde{H}_i), \tag{5}$$

where $\tilde{H}_i = Jx \sum_{i=1}^N S_i + \frac{K}{2} \sum_{i=1}^N S_i S_{i+1} + \frac{\Delta}{2} \sum_{i=1}^N S_i^2 S_{i+1}^2$. With the help of the transfer matrix method, the partition function can be deduced in the following form:

$$Z = \sqrt{\frac{\beta J N}{2\pi}} \int_{-\infty}^{\infty} dx \cdot e^{-\frac{\beta J N}{2} x^2} \cdot \text{Tr} \{ \mathbf{M}^N \}, \tag{6}$$

where \mathbf{M} is the transfer matrix which reads

$$\mathbf{M} = \begin{pmatrix} \exp(-\beta Jx + \frac{\beta K}{2} + \frac{\beta \Delta}{2}) & \exp(-\frac{\beta Jx}{2}) & \exp(-\frac{\beta K}{2} + \frac{\beta \Delta}{2}) \\ \exp(-\frac{\beta Jx}{2}) & 1 & \exp(\frac{\beta Jx}{2}) \\ \exp(-\frac{\beta K}{2} + \frac{\beta \Delta}{2}) & \exp(\frac{\beta Jx}{2}) & \exp(\beta Jx + \frac{\beta K}{2} + \frac{\beta \Delta}{2}) \end{pmatrix} \tag{7}$$

and $\text{Tr} \{ \mathbf{M}^N \}$ denotes the trace of the matrix \mathbf{M}^N that is expressed as

$$\text{Tr} \{ \mathbf{M}^N \} = \lambda_1^N + \lambda_2^N + \lambda_3^N. \tag{8}$$

In the thermodynamic limit ($N \rightarrow \infty$), the contribution of the other eigenvalues can be neglected except the

largest one $\lambda_m = \max(\lambda_1, \lambda_2, \lambda_3)$. Finally, the partition function of the system can be written as

$$Z = \sqrt{\frac{\beta J N}{2\pi}} \int_{-\infty}^{+\infty} dx \cdot e^{-N\beta \tilde{f}(\beta, x)}, \tag{9}$$

where $\tilde{f}(\beta, x) = \frac{J}{2}x^2 - \frac{1}{\beta} \ln \lambda_m(x)$. Moreover, the free energy per spin (the free energy density) is

$$f(\beta) = \min_x \left(\frac{J}{2}x^2 - \frac{1}{\beta} \ln \lambda_m(x) \right). \tag{10}$$

It is noteworthy that for given parameters K and Δ , the free energy per spin takes to the minimum value when x equals the magnetization m in Eq. (10). Therefore, ferromagnetic and stripe ferromagnetic phase can be distinguished by the magnetization m . An equilibrium state with m approaching 1 refers to a ferromagnetic one, while the magnetization of a stripe ferromagnetic state is close to a half.

3 Results

In this section, we discuss the ground states and the phase diagrams of the extended NK model. The phase diagrams are all shown in the two-dimensional (K, T) plane for different parameters Δ . Since the nearest-neighbor biquadratic coupling is an additional one in the extended model, it is an effective way to fix Δ and compare with the original one ($\Delta = 0$) in the same two-dimensional (K, T) plane to gain a better understanding of the various structures of PTs.

3.1 Ground state

The ground state is equivalent to the equilibrium state at zero temperature ($T = 0$), which can be expressed as a function of parameters in the Hamiltonian and the order parameters. The investigation of the ground states is rather significant, as it might provide valuable hints for further study of the phase transitions and diagrams. According to the Hamiltonian given by Eq. (2), one can easily determine the spin configurations of the ground states for different parameters K and Δ which correspond to the minimum of the energy per spin ε .

The result of the ground states includes three different types of phases. The ferromagnetic phase **F** refers to all spins pointing upward ($S_i = 1, \forall i$) or downward ($S_i = -1, \forall i$), and the energy per spin is $\varepsilon_{\mathbf{F}} = -\frac{J}{2} - \frac{K}{2} - \frac{\Delta}{2}$. Alternate pointing of nearest-neighbor spins appears in the antiferromagnetic state **AF** and its energy per spin is $\varepsilon_{\mathbf{AF}} = \frac{K}{2} - \frac{\Delta}{2}$, as the contribution of the first long-range coupling vanishes. Moreover, the stripe ferromagnetic state **SF** occurs when spins taking the value as ± 1 and 0 are alternately arranged (e.g. $S_{2i} = 0$ and $S_{2i+1} = \pm 1$ or $S_{2i} = \pm 1$ and $S_{2i+1} = 0, \forall i$), and it holds the constant energy

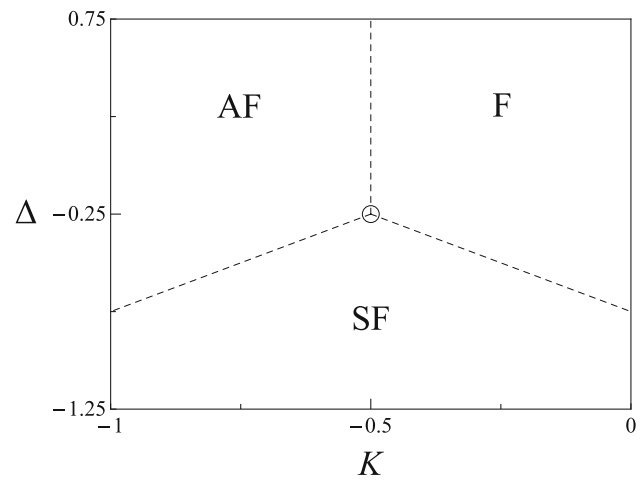


Fig. 1 Diagram of the ground state in the (K, Δ) plane. The respective corresponding ground state of each region has been indicated by letters in the margin, while three lines distinguishing the ground state intersect at the triple point represented by the hollow circle

per spin $\varepsilon_{\mathbf{SF}} = -\frac{J}{8}$, which is lower than that of the paramagnetic state ($S_i = 0, \forall i$ and $\varepsilon_{\mathbf{P}} = 0$).

The result of ground state in the extended NK model is shown in Fig. 1. The system has only two ground states **AF** and **F** with regard to different K when Δ takes a higher values ($\Delta > -0.25$), which is the same as the ordinary NK model. However, the additional ground state **SF** appears for a lower value of Δ ($\Delta < -0.25$). It may result in two intersections of the phase transition line and zero temperature line ($T = 0$) in one phase diagram.

3.2 Phase diagram

3.2.1 $\Delta < \Delta_1 = -0.25$

The structure of the phase diagram for Δ larger than $\Delta_1 = -0.25$ in this region has two separate phase transition lines. The ground states shown in Fig. 1 corroborate the phenomenon, as there are three different ground states in this range of Δ . We analyze this case by showing the phase diagram in Fig. 2 for $\Delta = -2$ as an example. When $T = 0$, the system first experiences a first-order phase transition from an antiferromagnetic state **AF** to a stripe ferromagnetic one **SF**, and then to a ferromagnetic state **F**, by increasing K . For the left transition line, it changes from a first-order phase transition line into a second-order one as T increases after passing the canonical tricritical point (CTP). The left transition line has the same form as that of the ordinary NK model, apart from a little difference close to $(K = -2.25, T = 0)$ (the transition point of ground states **AF** and **SF**) which is to be discussed later. As for the right transition line denoted by red solid line in the figure, it indicates that a small-scale first-order phase transition starting at $T = 0$ ends at a critical point (CP). This line separates the two ferromagnetic states

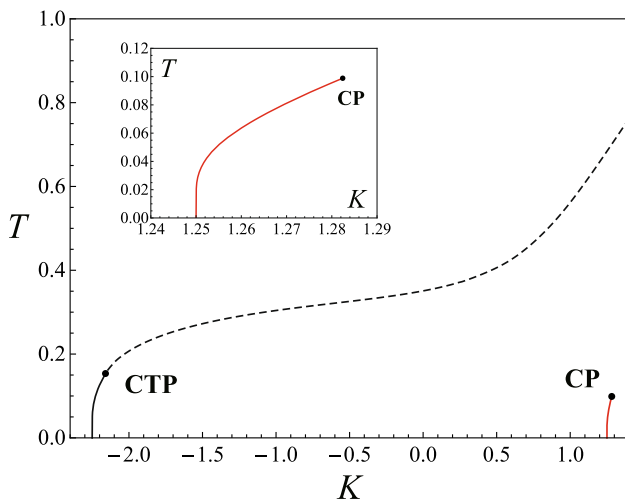


Fig. 2 (K, T) phase diagram of the extended NK model in the canonical ensemble with $\Delta = -2.0$. Solid and dashed lines denote the first- and second-order PT lines, respectively, in this and the other phase diagrams. The second-order transition line ends at the canonical tricritical point (CTP), while the first-order transition line between two ferromagnetic states ends at the critical point (CP)

SF and **F**. Due to the existence of the critical point and the absence of usual second-order phase transition paths, the transition between **SF** and **F** can be continuous in the magnetization, as paths can connect the two states without intersecting the red first-order phase transition line in the (K, T) plane. The coordinates of significant points for $\Delta = -2$ are: the canonical tricritical point ($K \simeq -2.160, T \simeq 0.154$) and the critical point ($K \simeq -1.282, T \simeq 0.099$).

The overall trends of the transition lines' movement are also worth analyzing, as shown in Fig. 3a. Along with Δ increases, the typical structure of the phase diagram is preserved in this region $\Delta < \Delta_1$ despite that the second-order transition line becomes steeper. Additionally, the two separate lines (left and right) move closer to the center $K = -0.5$. Phase diagrams show that the two lines meet together in the next region.

Another property that deserves analysis of the PT lines is re-entrant phase transition, which appears close to the transition point of the ground state **AF** and **SF**. Fig. 3b exhibits a typical re-entrant phase transition. When $-0.517 \simeq K_r < K < -0.5$, the system undergoes two phase transitions from **AF** to **SF** and to **AF** again by increasing T . In fact, the first-order re-entrant phase transition exists for $\Delta < \Delta_r \simeq -0.2192$, whereas its structure is not the same in different types of phase diagram for Δ in other regions. So in this region of Δ , all the left first-order transition lines contain a re-entrant phase transition segment, though it may be not obvious in phase diagrams for smaller Δ .

3.2.2 $-0.25 = \Delta_1 \leq \Delta \leq \Delta_2 \simeq -0.2188$

In this region, the phase diagram becomes more complicated with the existence of a triple point (TP). The behavior changes at the boundary value $\Delta = \Delta_1 =$

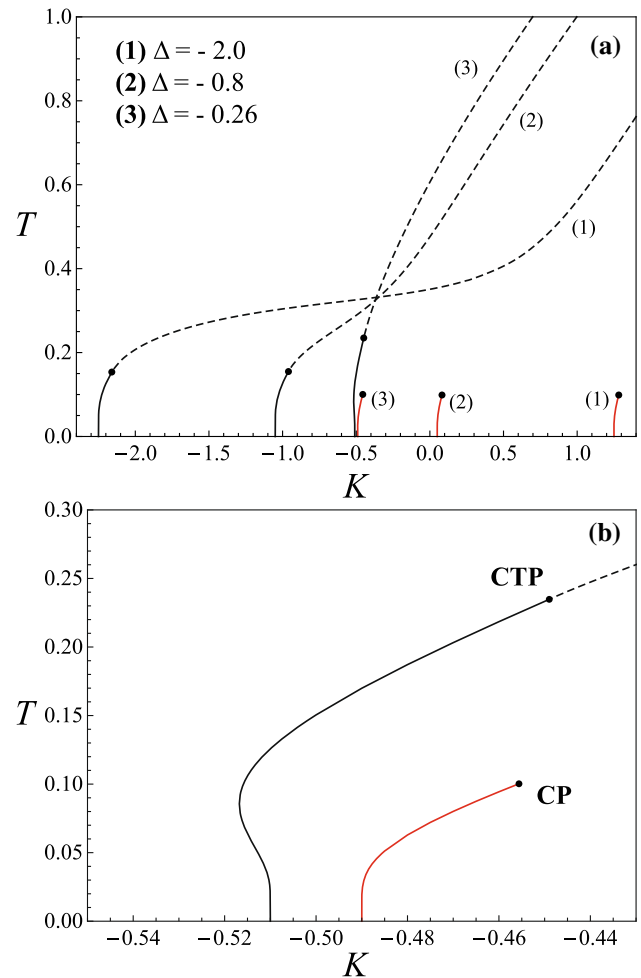


Fig. 3 **a** (K, T) phase diagram of the extended NK model corresponding to three values of Δ : $-2.0, -0.8, -0.26$, respectively. The black solid dots at the end of three red transition lines are critical points (CP) and the others are canonical tricritical points (CTP), related to different Δ . **b** Partial enlargement of the phase diagram for $\Delta = -0.26$. Re-entrant phase transition can be seen clearly on the left first-order phase transition line

-0.25 (Fig. 4a), where the ground state is a triple point and the two first-order phase transition lines, converge exactly there.

For Δ larger than the boundary, we choose $\Delta = -0.23$ as a sample case to illustrate the rich features of the system in this region. As shown in Fig. 4b, the first-order line starts at $(K = -0.5, T = 0)$ and bifurcates at the triple point (TP). The inset in Fig. 4b shows the regional enlargement near the triple point. The right red branch of the two first-order lines terminates at the critical point (CP), while the other, as before, ends at the canonical tricritical point (CTP) where it meets the second-order line. The coordinates of relevant points for $\Delta = -0.23$ are: the canonical tricritical point ($K \simeq -0.428, T \simeq 0.255$), the triple point ($K \simeq -0.496, T \simeq 0.084$) and the critical point ($K \simeq -0.484, T \simeq 0.102$).

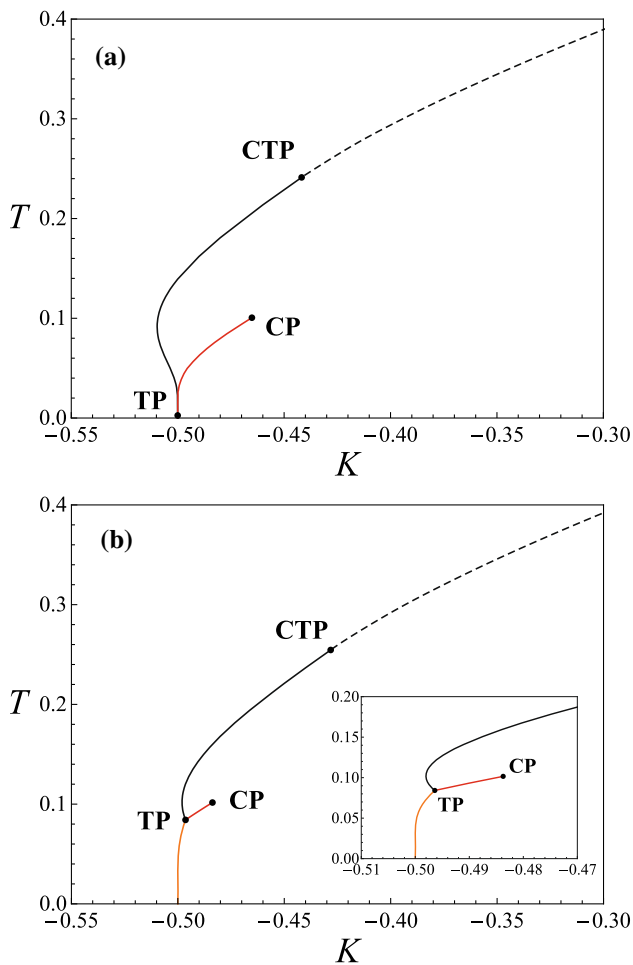


Fig. 4 (K, T) phase diagram of the extended NK model in the canonical ensemble. **a** $\Delta = -0.25$; **b** $\Delta = -0.23$, three phase transition lines near the triple point (TP) is further zoomed in the inset

For some specific situation like $K = -0.497$, the system undergoes three phase transitions when the temperature increases. The plots of the magnetization m as a function of temperature T and the temperature T as a function of the energy per spin ϵ can give a better demonstration. It can be seen in Fig. 5a that the magnetization steps are from close to 1 (ferromagnetic state **F**) to 0, then jump to different values near 0.6 (stripe ferromagnetic state **SF**) and go back to 0 finally, with T increasing. The canonical caloric curve is shown in Fig. 5b where red horizontal lines denote three phase transitions of the system. Since all phase transitions are first order, the magnetization changes abruptly and the energy jumps in the caloric curve.

As Δ gets larger, the triple point (TP) moves up to the right and the critical point (CP) to the left and down in the (K, T) plane. When Δ reaches the other boundary value $\Delta_2 \simeq -0.2188$, the two meet in one point.

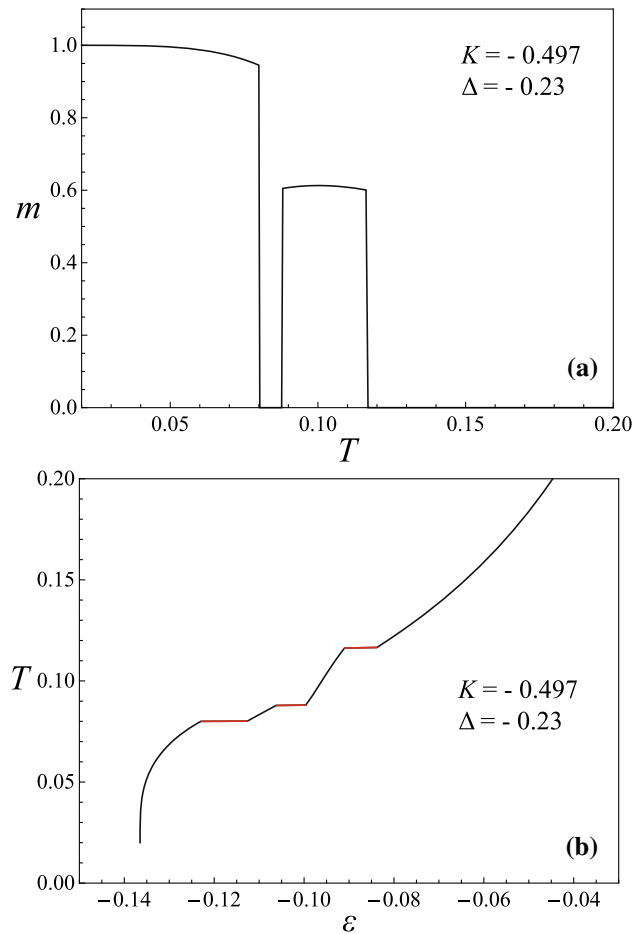


Fig. 5 Two canonical curves for $\Delta = -0.23$ and $K = -0.497$. **a** The magnetization m vs. the temperature T . **b** The temperature T vs. the energy per spin ϵ

3.2.3 $\Delta > \Delta_2 \simeq -0.2188$

In this range of Δ , the phase diagram is normal and similar to that of the ordinary NK model. As shown in Fig. 6, the position of the first- and second-order phase transition lines and the canonical tricritical points (CTP) vary depending on different Δ , while the phase diagram has the same form apart from that. By increasing Δ , both the two transition lines move upward. Moreover, the first-order transition line always starts at $(K = -0.5, T = 0)$, which is determined by ground state shown in Fig. 1.

4 Conclusion

In this paper, we have studied the extended spin-1 Nagle-Kardar model with an additional nearest-neighbor biquadratic coupling. The partition function

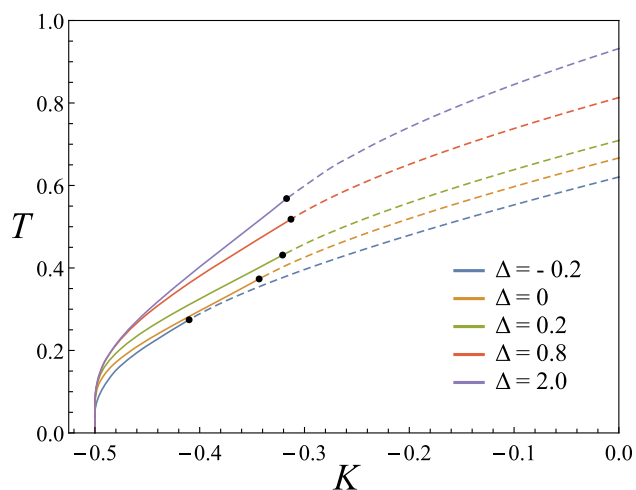


Fig. 6 (K, T) phase diagram of the extended NK model corresponding to different values of Δ : -0.2 , 0 , 0.2 , 0.8 , 2.0 respectively. Black solid dots at the intersection of first- and second-order transition lines are the canonical tricritical points (CTP)

of the model and various properties in the phase transitions and phase diagrams pertaining to the canonical ensemble have been investigated analytically. Though the phase diagram should be represented in 3—dimensional plane for two changeable parameters in the Hamiltonian, we fix the value of nearest-neighbor biquadratic coupling parameter Δ for the sake of convenience and better comparison with the ordinary NK model.

Three regions are separated by Δ based on the characteristics of the phase transition and phase diagram. For $\Delta < \Delta_1 = -0.25$, the phase diagram has two separate transition lines. One of them has the structure similar to that of the ordinary model except for the re-entrant phase transition near the transition point of two ground state **AF** and **SF**, while the other one is a simple first-order phase transition line. When $-0.25 = \Delta_1 \leq \Delta \leq \Delta_2 \simeq -0.2188$, the triple point connecting three different first-order lines exists in the phase diagram and re-entrant phase transition remains. Thus, the system can undergo three phase transitions for specific parameters while T increases. The phase diagram has the same form as that of the ordinary model for $\Delta > \Delta_2 \simeq -0.2188$, since the extra first-order transition line disappears.

In summary, the additional nearest-neighbor biquadratic interaction in the Hamiltonian has a significant effect on the system compared to the ordinary NK model. The two most prominent and distinctive phenomena of the new system are the new stripe ferromagnetic state and re-entrant phase transition. In the Hamiltonian, the antiferromagnetic nearest-neighbor coupling distinguishes between the spins pointing upward or downward. However, the contribution to the biquadratic interaction of the two non-zero spins is the same in the spin-1 system. Therefore the difference between the two short-range interactions gener-

ates the new state and complex phase transitions in the first and second ranges of Δ . For Δ in the third range, the impact of the biquadratic interaction is fading and the system gradually resembles the original one, as the sum of squared terms is non-negativity in the added coupling. In terms of re-entrant phase transition, the range of parameters in the Hamiltonian corresponding to the occurrence of re-entrance is quite narrow and usually difficult to be observed. A rough estimate is that the re-entrant phase transition no longer occurs when $\Delta > -0.219$.

The new model leads to a better general understanding of competition with different forms of interactions at different scales. We can believe that in higher dimensional spin lattices the additional coupling and corresponding extended NK model will present richer phase behaviors. Moreover, it would be quite interesting to consider the solution of the extended model in the microcanonical ensemble and on the spin- S case where S is higher than one.

Author contributions

This project was conducted under Dr. J-XH's supervision. J-TY wrote the paper. Both authors carried out the calculation, were involved in the discussion of results, and have read and approved its final version.

Data availability statement This manuscript has no associated data or the data will not be deposited. [Authors' comment: The data reported in the paper are available from the corresponding author on reasonable request.]

References

1. L.D. Landau, E.M. Lifshitz, *Statistical Physics* (Elsevier, London, 2013)
2. J. Sethna, *Statistical Mechanics: Entropy, Order Parameters, and Complexity* (Oxford University Press, New York, 2021)
3. H. Nishimori, G. Ortiz, *Elements of Phase Transitions and Critical Phenomena* (Oxford University, Oxford, 2010)
4. R.K. Pathria, *Statistical Mechanics* (Elsevier, London, 2022)
5. M.W. Zemansky, R.H. Dittman, *Heat and Thermodynamics: An Intermediate Textbook* (McGraw-Hill, New York, 1997)
6. J.-X. Hou, Eur. Phys. J. B **94**, 6 (2021)
7. J.-X. Hou, Phys. Rev. E **104**, 024114 (2021)
8. J.-X. Hou, Eur. Phys. J. B **94**, 151 (2021)
9. V.V. Hovhannisyanyan, N.S. Ananikian, A. Campa, S. Ruffo, Phys. Rev. E **96**, 062103 (2017)
10. M. Seul, D. Andelman, Science **267**, 476 (1995)
11. U. Löw, V. Emery, K. Fabricius, S. Kivelson, Phys. Rev. Lett. **72**, 1918 (1994)
12. O.D.R. Salmon, J.R. de Sousa, M.A. Neto, Phys. Rev. E **92**, 032120 (2015)

13. O.D.R. Salmon, J.R. de Sousa, M.A. Neto, I.T. Padilha, J.R.V. Azevedo, F.D. Neto, *Physica A* **464**, 103 (2016)
14. O.D.R. Salmon, M.A. Neto, F.D. Neto, D.A.M. Pariona, J.R. Tapia, *Phys. Lett. A* **382**, 3325 (2018)
15. A. Campa, G. Gori, V. Hovhannisyan, S. Ruffo, A. Trombettoni, *J. Phys. A* **52**, 344002 (2019)
16. V.V. Prasad, A. Campa, D. Mukamel, S. Ruffo, *Phys. Rev. E* **100**, 052135 (2019)
17. T. Dauxois, P. de Buyl, L. Lori, S. Ruffo, *J. Stat. Mech.* P06015 (2010)
18. O. Cohen, V. Rittenberg, T. Sadhu, *J. Phys. A Math. Theor.* **48**, 055002 (2015)
19. E. Albayrak, *Mod. Phys. Lett. B* **35**, 2150286 (2021)
20. F. Litaiff, J.R. de Sousa, N.S. Branco, *Solid State Commun.* **147**, 494 (2008)
21. A. Campa, T. Dauxois, S. Ruffo, *Phys. Rep.* **480**, 57 (2009)
22. T. Dauxois, S. Ruffo, E. Arimondo, M. Wilkens, *Dynamics and Thermodynamics of Systems with Long Range Interactions* (Springer, Berlin, 2002)
23. J.-X. Hou, *Phys. Rev. E* **99**, 052114 (2019)
24. J.-X. Hou, *Eur. Phys. J. B* **93**, 82 (2020)
25. Z.-Y. Yang, J.-X. Hou, *Phys. Rev. E* **101**, 052106 (2020)
26. Z.-X. Li, Y.-C. Yao, S. Zhang, J.-X. Hou, *Mod. Phys. Lett. B* **34**, 2050318 (2020)
27. S.-Y. Jiao, J.-X. Hou, *Mod. Phys. Lett. B* **35**, 2150095 (2021)
28. J.-X. Hou, *Mod. Phys. Lett. B* **36**, 2150621 (2022)
29. Y.-C. Yao, J.-X. Hou, *Physica A* **590**, 126776 (2022)
30. Z.-Y. Yang, J.-X. Hou, *Phys. Rev. E* **105**, 014119 (2022)
31. J.F. Nagle, *Phys. Rev. A* **2**, 2124 (1970)
32. M. Kardar, *Phys. Rev. B* **28**, 244 (1983)
33. D. Mukamel, S. Ruffo, N. Schreiber, *Phys. Rev. Lett.* **95**, 240604 (2005)
34. Y.-C. Yao, J.-X. Hou, *Int. J. Theor. Phys.* **60**, 968 (2021)
35. J.C. Bonner, J. Nagle, *J. Appl. Phys.* **42**, 1280 (1971)
36. M. Kaufman, M. Kahana, *Phys. Rev. B* **37**, 7638 (1988)
37. M. Mézard, G. Parisi, M.A. Virasoro, *Spin Glass Theory and Beyond: An Introduction to the Replica Method and its Applications* (World Scientific, Singapore, 1987)
38. S. Redner, *J. Stat. Phys.* **25**, 15 (1981)
39. R.R. Singh, Z. Weihong, C. Hamer, J. Oitmaa, *Phys. Rev. B* **60**, 7278 (1999)
40. O. Sushkov, J. Oitmaa, Z. Weihong, *Phys. Rev. B* **63**, 104420 (2001)
41. N. Shannon, B. Schmidt, K. Penc, P. Thalmeier, *Eur. Phys. J. B* **38**, 599 (2004)
42. M. Spenke, S. Guertler, *Phys. Rev. B* **86**, 054440 (2012)
43. L. Wang, A.W. Sandvik, *Phys. Rev. Lett.* **121**, 107202 (2018)
44. H. Li, L.-P. Yang, *Phys. Rev. E* **104**, 024118 (2021)
45. M. Blume, V. Emery, R.B. Griffiths, *Phys. Rev. A* **4**, 1071 (1971)
46. N. Branco, *Phys. Rev. B* **60**, 1033 (1999)
47. C.E. Fiore, V.B. Henriques, M.J. de Oliveira, *J. Chem. Phys.* **125**, 164509 (2006)
48. L.J. de Jongh, W.D. van Amstel, A.R. Miedema, *Physica* **58**, 277 (1972)
49. G. Chapuis, G. Brunisholz, C. Javet, R. Roulet, *Inorg. Chem.* **22**, 455 (1983)
50. J. Rossat-Mignod, P. Burllet, H. Bartholin, O. Vogt, R. Lagnier, *J. Phys. C Solid State Phys.* **13**, 6381 (1980)
51. G. Ódor, *Rev. Mod. Phys.* **76**, 663 (2004)

Springer Nature or its licensor (e.g. a society or other partner) holds exclusive rights to this article under a publishing agreement with the author(s) or other rightsholder(s); author self-archiving of the accepted manuscript version of this article is solely governed by the terms of such publishing agreement and applicable law.